Original Research Article

Design of novel coumarin derivatives inhibitors of monoamine oxidase B (MAO_B) by the QSAR model.

Abstract

We report here the model serving as a research tool essential to the screening of a new COU inhibitor complex formation. In three-dimensional format, the enzyme inhibitors of COUs were made by end-to-end modification in the crystal protein 7-(3-chlorobenzyloxy)-4-(methylamino) methyl-coumarin co-crystallized (Whose crystallographic data entry code is 2v61). Where we chose 29 COUs as a training game with the knowledge of their experimental inhibitory activity (IC_{50}^{exp}). Above all, we have established the gas phase model QSAR. Then, to achieve an alignment of the enthalpies of complex formation of each coumarin derivative with their experimental inhibitory activity IC_{50}^{exp}. In addition, the solvent effect and loss of inhibitor entropy in the complex gave a high QSAR model of with a linear correlation of GFE ($\Delta\Delta G_{com}$) of MAO-B – COUs complex formation and IC50exp ($pIC_{50}^{exp} = -0.22.\Delta\Delta G_{com} + 7.73$; $R^2 = 0.93$), which was subsequently confirmed from the PH4 3D-QSAR model. This method of investigation allowed us to obtain an analogue COU, whose predicted activity is better (IC_{50}^{pre} of 20 pM). QSAR by complexation remains a reliable and robust method for achieving a high activity candidate.

Comment [A1]: Abstract should be rewritten.
Lack of understanding
Should state the limitation which the present work fulfills.
Grammatical errors & inappropriate sentence formation.

KEYWORDS

Coumarin inhibitors; human monoamine oxidase B (*h*MAO-B); coumarins derivatives (COUs); quantitative structure-activity relationships (QSAR); pharmacophore (PH4); molecular modeling.

1. INTRODUCTION

Monoamine oxidase (MAO, EC.1.4.3.4, amine-oxygen oxidoreductase) is a membrane-bound flavoenzyme responsible for the oxidative deamination of xenobiotic amines [1] and monoamine neurotransmitters such as serotonin (5-HT), norepinephrine (NE), and dopamine (DA) [2]. The enzyme exists in two forms, *h*MAO-A and *h*MAO-B, encoded by different genes and differing in tissue distribution, structure and substrate specificity [3]. By inhibiting *h*MAO, the degradation of monoamines is blocked, leading to an increase in their availability for their physiological fonctions. In keeping with these premises, the development of *h*MAO inhibitors has led to important break-throughs in the therapy of several neuropsychiatric disorders [4].

In recent years, interest in selective *h*MAO-B inhibitors has increased significantly due to the discovery that expression levels of this isoenzyme in neuronal tissue increase 4-fold with age, resulting in an increment of dopamine metabolism, as well as of production of hydrogen peroxide, causative of oxidase stress and may play a relevant role in the etiology of neurodegenerative diseases [5]. As a result, MAO-B inhibitors would useful as adjuvant for the treatment of Parkinson's disease. Crystal structures revealed that residues Ile199 [6, 7] and Tyr326 [8] specifically and catalytically, are important for ligand binding. The aromatic cage delimited by Tyr398 and Tyr435 plays a key role in coordinating ligands in the active site to the FAD molecule [9]. Several different MAO-B inhibitors are used against Parkinson's disease, including [10]: selegiline hydrochloride (tablets, orally disintegrating tablet), rasagiline (tablet) and safinamide (tablet).

The irreversible inhibitors of MAO-B, selegiline and rasagiline, are used clinically in treatment of Parkinson's disease, and a recently introduced reversible MAO-B inhibitor, safinamide, has also been shown to be effective. Modification of the pharmacokinetic characteristics of these inhibitors has led to development of new drug form against Parkinson's disease.

In this study we focused on validating the binding modes of a series of 33 coumarin derivatives (COU) with reported experimental MAO-B inhibitory activity in the nanomolar range [11], the most active of which is the endogenous ligand of the deposited RX crystallography structure in complex with MAO-B (PDB code 2V61). From a training set (TS) of 29 coumarin derivatives (COU1-29) and a validation set of 4 COU30-33, a one descriptor QSAR model of MAO-B inhibition was built by *in situ* modification of the reference inhibitor COU1 in the above mentioned 3D structure 2v61.pdb in the gas phase and in the solvent taking account of biological medium solvation. This model correlates the relative Gibbs free energy (rGFE) of MAO-B – COU1-30 complex formation with observed (IC_{50}^{exp}). A 3D pharmacophore (PH4) was generated from the QSAR identified active conformation of COUs in order to screen the coumarins COUs chemical subspace for novel COUs analogues with predicted better potency and favorable pharmacokinetic profile.

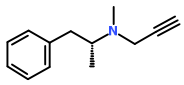

Selegiline (IC_{50} = 6.8 nM, [12])

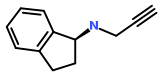

Rasagiline (IC_{50} = 14 nM)

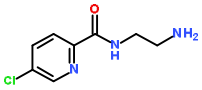

Lazabemide (IC_{50} = 30 nM [13])

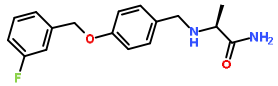

Safinamide (K_i = 0,45 µM, [14])

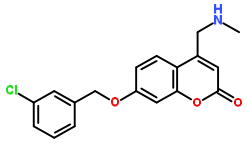

7-[(3-chorobenzyl)oxy]-4-[(methylamino)-methyl]-2H-chromen-

2-one methanesulfonate (COU1, IC_{50}^{exp} = 13 nM, [11])

2. MATERIALS AND METHODS

2.1. Training sets

Structural studies and bioassays (IC_{50}^{exp}) of our studied coumarin derivatives (COU) MAO-B inhibitors were retrieved from P. Leonardo *et al.* [11]. The efficacy range of inhibitory concentrations (13≤ IC_{50}^{exp} ≤ 16,100 nM), allows us to realize QSAR models. The whole series of 33 COUs were divided into a training (TS) and a validation (VS) sets of 29 and 4 COUs respectively. [11].

2.2. Model building

The entire complex (E:I), with free MAO-B (E) and inhibitor (I) was resolved to a reliability factor of 1.7 Å containing the 7-[(3-chorobenzyl)oxy]-4-[(methylamino)-methyl]-2H-chromen-2-onemethanesulfonate (COU1) bound to MAO-B (Whose crystallographic data entry code 2v61 [15]) from Discovery Studio 2.5 software. [16].Virtual design plan to result in new COU analogues with higher predicted activity is presented in scheme1. The structures (E and E : I complexes) were at the neutral pH=7 and neutral N- and C-terminal residues, all protonizable and ionizable aminoacids being charged, without any crystallographic water molecules. The inhibitors were built into the 2v61 structure by *in situ* replacing derivative groups of the COU1 moiety followed by systematic conformational search of the replacing group coupled with a careful energy-minimization of the modified inhibitor and surrounding MAO-B active site residues [17, 18, 19, 20, 21, 22, 23, 24, 25, 26, 27, 28, 29, 30, 31, 32].

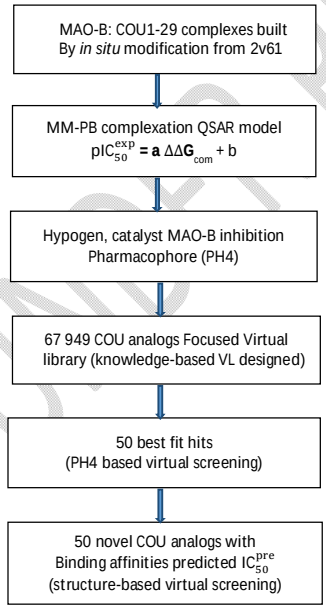

Scheme 1.Virtual design plan to result in new COU analogues with higher predicted

2.3. MOLECULAR MECHANICS

Molecular mechanics, a fundamental method of our work has been previously described by [21,33]

2.4. Conformational search

For conformational research we recommend reading the following articles [16, **Error! Bookmark not defined.**, **Error! Bookmark not defined.**].

2.5. Solvation Gibbs free energies

As for the free solvation energy has been perfectly described by the following articles [**Error! Bookmark not defined.**,**Error! Bookmark not defined.**,34,34,35,36,37].

2.6. CALCULATION OF BINDING AFFINITY AND QSAR MODEL

The methods for exploring the QSAR and the binding affinity have been described by the articles whose references are [15,16,38]:

2.7. Interaction energy

Interaction energy is a priority of our method. But to deepen your knowledge on this part we refer you to the articles cited below [16,**Error! Bookmark not defined.**, 33].

2.8. Pharmacophore generation

The pharmacophore generation from active conformation of COU1-29 from the 3D QSAR pharmacophore protocol by catalyst HypoGen algorithm [39] implemented in Discovery Studio [16] has been fully described formerly [30].

3-RESULTS AND DISCUSSION

We selected 29 COUs as a training set and 4 COUs as a validation set (Table 1) designed from the same laboratory with their given inhibitory activity. [11]. All of our compounds were generated by substitutions on the R1 and R2 groups of the coumarin derivative scaffold, as shown in Table 1. Their experimental inhibitory activity IC_{50}^{exp} has a significant gap to build a reliable model of COU inhibitor.

Comment [A2]: References to be cited in order.

Comment [A3]: References to be cited in order.

Comment [A4]: Along with references cited , the method should be described in brief.

Comment [A5]: Inappropriate with langauage issues & no briefings.

Table 1. Composition of the COUs series, training set and validation set [11] are used to base the QSAR of inhibitors binding. Substituants R1 and R2 are numbered in the table as group index #R≡.group index.

Comment [A6]: Each table should be separated with different captions.

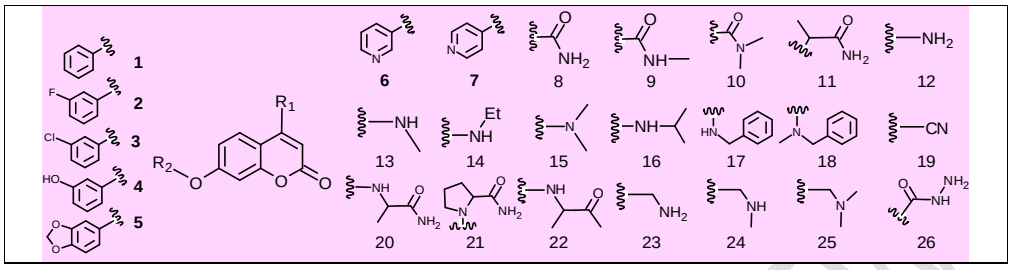

Training set	COU1	COU2	COU3	COU4	COU5	COU6	COU7	COU8	COU9	COU10	COU11	COU12
#R_1–#R_2	13–3	9–1	13–2	13–5	12–1	9–3	13–1	8–3	26–1	10–3	8–2	26–3
K_i (nM)	13	15	18	20	21	24	28	30	40	40	50	90

Training set	COU13	COU14	COU15	COU16	COU17	COU18	COU19	COU20	COU21	COU22	COU23	COU24
#R_1–#R_2	14–2	11–1	11–2	8–1	20–3	19–1	23–3	24–3	15–2	15–3	6–1	20–1
K_i (nM)	100	100	100	200	210	230	250	300	510	1120	1300	1800

Training set	COU25	COU26	COU27	COU28	COU29
#R_1–#R_2	7–1	17–3	18–3	21–3	21–1
K_i (nM)	2000	3600	8000	9600	16100

Validation set	COU30	COU31	COU32	COU33
#R_1–#R_2	16–2	25–1	8–4	10–1
K_i (nM)	3800	460	1000	400

3.1. Quantitative Structure-Activity Relationships model

The GFE of the MAOB-COU1 complex was used to build the QSAR model. See (Fig. 1) in the site we carried out end-to-end modification of the R1 and R2 fragments if possible to achieve compounds from the test set and the validation set.
The link to our database is as follows: (PDB entry code 2v61 [15]). Table 2 provides us with information on the molecular masses, the enthalpy in the gaseous medium, the enthalpy in the solvated medium with their inhibitory activity respectively of our compounds of coumarins derivatives inhibitors [11].

Our model establishes a link between inhibitory activity and the $\Delta\Delta G_{com}$ [11]. First the exploratory model in gas phase pIC_{50}^{exp} =f ($\Delta\Delta H_{MM}$) and the deepest insight model (solvation and inhibitor vibrational entropy loss) pIC_{50}^{exp} =f ($\Delta\Delta G_{com}$) all in Table 3 and Figure 2. Statistical data such as determination coefficient and Fischer F-test suggest strong connection between the binding model and pIC_{50}^{exp} of COUs.

Table 2. Complexation Gibbs free energy (binding affinity) and its components for the training set (TS) of MAO-B inhibitors COU1-29 and validation set (VS) inhibitors COU30-33.

Training set[a]	M_w[b]	$\Delta\Delta H_{MM}$[c]	$\Delta\Delta G_{sol}$[d]	$\Delta\Delta TS_{vib}$[e]	$\Delta\Delta G_{com}$[f]	IC_{50}^{exp}[g]
COU1	329	0	0	0	0	13
COU2	323	0.07	1.91	1.95	0.03	15
COU3	313	0.78	0.38	0.43	0.74	18
COU4	339	0.93	-1.23	-1.14	0.84	20
COU5	281	1.32	-0.63	0.73	-0.04	21
COU6	357	-0.91	2.27	0.10	1.25	24
COU7	295	2.81	0.87	2.41	1.27	28
COU8	343	0.12	1.25	-1.79	3.17	30
COU9	324	2.03	0.40	2.07	0.35	40
COU10	371	-0.13	0.27	-2.83	2.98	40
COU11	327	1.38	0.54	-1.44	3.36	50
COU12	358	0.95	0.67	0.20	1.41	90
COU13	327	1.51	1.50	0.50	2.51	100
COU14	323	2.48	1.17	0.98	2.68	100
COU15	341	1.42	1.06	0.06	2.43	100
COU16	309	2.95	0.33	-0.24	3.52	200
COU17	372	0.70	1.65	-2.46	4.81	210
COU18	291	4.15	0.41	-0.12	4.69	230
COU19	329	0.66	2.37	-0.33	3.25	250
COU20	343	3.10	2.71	-0.20	6.01	300
COU21	327	2.00	1.29	-1.08	4.36	510
COU22	343	6.40	2.09	-0.72	9.22	1120
COU23	310	4.50	0.73	-3.10	8.33	1300
COU24	352	6.28	3.58	2.57	7.29	1800
COU25	310	4.94	2.55	-2.51	10.01	2000
COU26	405	6.71	3.70	-1.56	11.97	3600
COU27	419	9.49	0.45	-1.28	11.22	8000
COU28	398	6.69	5.88	0.47	12.09	9600
COU29	364	8.82	5.87	2.18	12.51	16100

Validation set	M_w [b]	$\Delta\Delta H_{MM}$ [c]	$\Delta\Delta G_{sol}$ [d]	$\Delta\Delta TS_{vib}$ [e]	$\Delta\Delta G_{com}$ [f]	$\frac{pIC_{50}^{pre}}{pIC_{50}^{exp}}$
COU30	341	9.14	1.53	0.91	9.76	1.029
COU31	323	5.29	1.13	1.44	4.97	1.046
COU32	325	3.41	1.69	-1.35	6.45	1.051
COU33	337	3.58	0.33	-1.16	5.07	1.032

[a] for the chemical structures of the training set of inhibitors see Table 1; [b] M_w (g/mol) is the molecular mass of inhibitors ; [c] $\Delta\Delta H_{MM}$ (kcal/mol) is the relative enthalpic contribution to the Gibbs free energy change related to enzyme-inhibitor (E:I) complex formation derived by molecular mechanics (MM): $\Delta\Delta H_{MM} \cong [E_{MM}\{E:I_x\} - E_{MM}\{I_x\}] - [E_{MM}\{E:I_{ref}\} - E_{MM}\{I_{ref}\}]$, I_{ref} is the reference inhibitor COU1; [d] $\Delta\Delta G_{sol}$ (kcal/mol) is the relative solvation Gibbs free energy contribution to the Gibbs free energy change of E:I complex formation: $\Delta\Delta G_{sol} = [G_{sol}\{E:I_x\} - G_{sol}\{I_x\}] - [G_{sol}\{E:I_{ref}\} - G_{sol}\{I_{ref}\}]$; [e] $\Delta\Delta TS_{vib}$ (kcal/mol) is the relative entropic contribution of inhibitor I_x to the Gibbs free energy related to E:I complex formation: $\Delta\Delta TS_{vib} = [\Delta\Delta TS_{vib}\{I_x\}_E - \Delta\Delta TS_{vib}\{I_x\}] - [\Delta\Delta TS_{vib}\{I_{ref}\}_E - \Delta\Delta TS_{vib}\{I_{ref}\}]$; [f] $\Delta\Delta G_{com} \cong \Delta\Delta H_{MM} + \Delta\Delta G_{sol} - \Delta\Delta TS_{vib}$ (kcal/mol) is the relative Gibbs free energy change related to E:I_x complex formation; [g] IC_{50}^{exp} is the experimental half-maximal inhibitory concentration (in nM) obtained from reference [11]; [h] Ratio of predicted and experimental half-maximal inhibition concentrations $pIC_{50}^{pre}/pIC_{50}^{exp}$ ($pIC_{50}^{pre} = -\log_{10}IC_{50}^{pre}$) was predicted from computed $\Delta\Delta G_{com}$ using the regression equation shown in Table 3.

Table 3. Regression analysis of computed binding affinities $\Delta\Delta G_{com}$, its enthalpic component $\Delta\Delta H_{MM}$, and experimental IC_{50}^{exp} of coumarin derivatives (COUs) towards MAO-B: $pIC_{50}^{exp} = -\log_{10}(IC_{50}^{exp})$.

Statistical Data of Linear Regression	(A)	(B)
$pIC_{50} = -0.30 \times \Delta\Delta H_{MM} + 7.55$ **(A)**		
$pIC_{50} = -0.22 \times \Delta\Delta G_{com} + 7.73$ **(B)**		
Number of compound n	29	29
Square correlation coefficient of regression R^2	0.82	0.93
LOO cross-validated square correlation coefficient R^2_{xv}	0.81	0.93
Standard error of regression σ	0.40	0.24
Statistical significance of regression, Fisher F-test	120.5	375.1
Level of statistical significance α (%)	>95	>95
Range of activities IC_{50}^{exp} (nM)	13 – 16100	

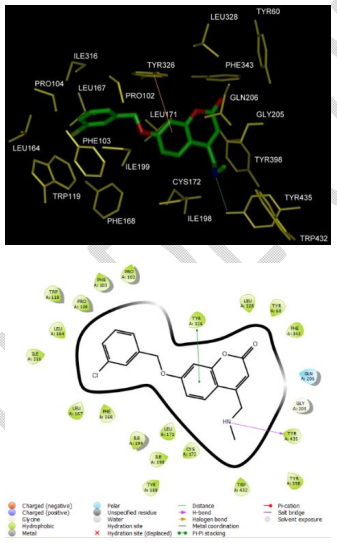

Figure 1. (Top) 3D schematic interaction diagram of the most potent inhibitor COU1 (Table 1) at the active-site of MAO-B protein; (Bottom) 2D structure of the active-site with bound inhibitor COU1.

The ratio $pIC_{50}^{pre}/pIC_{50}^{exp}$, with the pIC_{50}^{pre} computed with Equation (**B**), Table 3 for VS COU30-33 not in the TS, is near one attesting significant predictive capacity of the complexation QSAR model, Table 1 and 2.

3.2. Binding mode of inhibitors

In the crystal structure of MAO-B –COU1 [11] the substitution at R1-and R2-groups of the coumarin derivative scaffold of the inhibitor sits in a hydrophobic cavity of the active-site surrounded by side chains of predominantly nonpolar residues : Trp119, Leu164, Leu167, Phe168, Ile198, Ile199, Ile316 and Tyr326. While the R2-group at position 7 has preferred binding conformation in the hydrophobic cavity, at position 4 (R1) faces a steric hindrance giving the better affinity to smaller substituent confirmed by our QSAR model. All interactions observed in the crystal structure were conserved. As displayed in Fig. 1, the binding mode of COUs at MAO-B active site of the best active COU1 in 2D is supported by the following interactions: π-π stacking with Tyr326, hydrogen bond with Tyr435 and hydrophobic contacts. The MAO-B active site consists of two cavities, the substrate cavity in front of the flavin and the entrance cavity located underneath the protein surface [40,41]. Beside the robustness of the QSAR model, the analysis of the interactions between COUs and MAO-B is expected to reveal key interactions behind E-I affinity able to guide the selection of novel potency improving substituents through more intensive hydrogen bonds (HBs), Van der Waals (VdW), hydrophobic contacts.

We analyzed contributions of individual residues of the enzyme binding pocket to the total computed enzyme-inhibitor interaction energy (E_{int}). In the hydrophobic pochet we have noticed a significant contribution to the E_{int} from residues Trp119, Leu164, Leu167 Phe168, Ile198, Ile199, Ile316 and Tyr326. (Fig. 3).

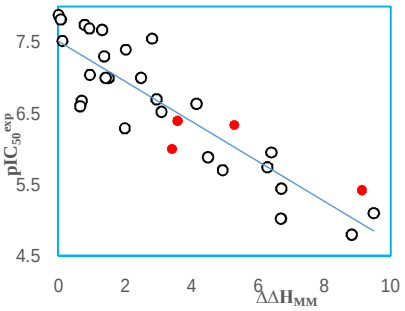

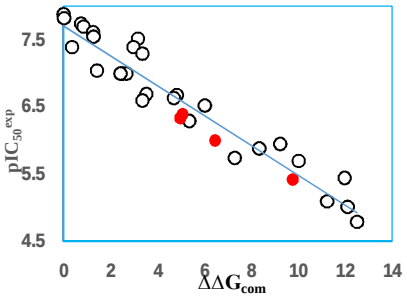

Figure 2. (Top) the equality curve of pIC_{50} and and the enthalpy of the coumarin series in the gaseous medium ($\Delta\Delta H_{MM}$) of MAOB-COUx complex formation.; (Below) similar plot for relative complexation Gibbs free energies of the MAOB-COUx complex formation $\Delta\Delta G_{com}$ of training set, all in kcal.mol^{-1}. Data from the validation set is shown in red; the black circles represent the COUs of the test sets.

3.3. Interaction Energy

in addition to the correlation curve, other structural information is obtained from the interaction energy diagram (IE, ΔE_{int}) obtained for each inhibitor in the test set. Analysis of the interaction energy is an important contribution to detecting the inhibitory power of each fragment with the residues at the active site. To carry out our comparative study of interaction energy diagrams, we decided to divide our series of COUs from the test game into three parts. See fig. 3 (compounds with higher inhibitory activities, those with medium activities and those with low activities). This comparison led us to identify residues that strongly contribute to the increase of the inhibitory power of each compound. Therefore, no suggestions for suitable substitutions able to improve the binding affinity emerge suggesting a combinatorial approach where novel COU analogs virtual library is enumerated from new R-group substituents and in silico screened with help of the PH4 pharmacophore of MAO-B inhibition derived from our complexation QSAR model. A reported alternative approach through steered Molecular Dynamics Stimulations has been reported revealing in a bilayer environment per-residue interaction energy for unfortunately reduced number of MAO-B inhibitors probably due to huge time consuming computations engaged just confirmed the key role of Tyr326, Leu169, Gln206, Tyr398, Asp318, already noticed from crystal structure [42].

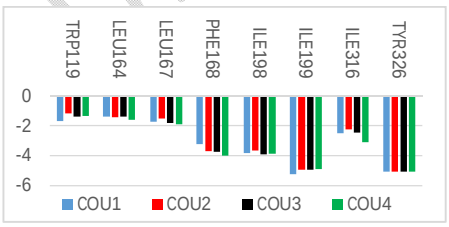

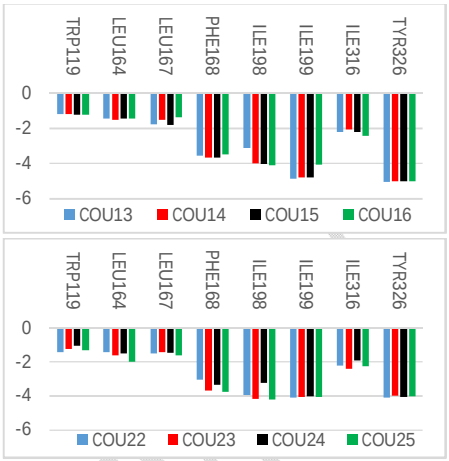

Figure 3. Mechanics intermolecular interaction energy E_{int} breakdown to residue contributions in the hydrophobic pochet [kcal.mol^{-1}]: (Top) two most active inhibitors COU1-2, (Middle) moderately active inhibitors COU14-15, (Bottom) less active inhibitors COU23-24. Table 2 [11].

3.4. Pharmacophore model of inhibitory activity

The 3D-QSAR PH4 pharmacophore generation process fully has been described previously [30]. The most active TS COU1 (IC_{50}^{exp} = 13nM and $IC_{50}^{exp} \leq$ 2 x 13 nM) alone served for features building and retained. The 10 optimized hypotheses with the lowest costs, 130.5 (Hypo1) to 176.4 (Hypo10) are the bests PH4 for IC_{50} prediction, higher than the fixed cost (89.9), lower than the null one (260.8) both separated by a gap Δ = 170.9, very >> 70 and synonymous of high predictability. The computational process for each hypothesis namely statistical significance, Fisher randomization, CatScramble programme were described earlier [30] and for S=98% the 10 lowest cost hypotheses built from COUs active conformation are listed in Table 4. Hypo 1 with the lowest cost (130.5), RMSD (1.575), highest R^2 (0.89) was retained as MAO-B inhibition PH4. The statistical data of hypotheses (costs, RMSD, R^2) and of the correlation plot pIC_{50}^{exp} vs pIC_{50}^{pred} in Figure 4 (pIC_{50}^{exp} = 0.75.pIC_{50}^{pre} + 1.66; n =29, R^2 =0.91, R_{xv}^2 =0.90, F-test = 288.3, σ =0.276, α > 95%, 1.575 ≤ RMSD ≤ 2.442, 0.72 ≤ R^2 ≤ 0.89) document a PH4 predictive power as robust as the MM-PB complexation QSAR model with $\Delta\Delta G_{com}$ as single descriptor. To validate the PH4 model, the ratio pIC_{50}^{pre} / pIC_{50}^{exp} for the validation set (VS, Table 1) of COU30: 1.126, COU31: 1.06, COU32: 0.998, COU33: 1.180 has been computed and the closeness to one attests its predictability. The geometry of the Hypo1 pharmacophore of MAO-B inhibition is displayed on Figure 4 with the appropriate features and their spatial coordinates. The configuration cost (9.4) << 17 the upper limit [43] also attests the PH4 quality. The use of the PH4 for virtual screening mostly is based on the inclusion of the hydrophobic feature (HYD, Figure 4) in the best PH4 model at the substitution position of the R_2 group.

Table 4. The variables derived from the pharmacophore generated from our series of the training set.

Hypothesis	RMSD [a]	R^{2} [b]	Total Costs [c]	Costs Diff.[d]	Closest Random[e]	Features f
Hypo1	1.575	0.89	130.5	130.3	185.2	HBA-LI, HBA-LI, HYD-Ar, Ar
Hypo2	1.777	0.86	138.0	122.8	192.9	HBA-LI, HBA-LI, HBA-LI
Hypo3	1.818	0.85	140.7	120.1	204.4	HBA-LI, HBA-LI, HYD-Ar
Hypo4	1.880	0.84	143.3	117.5	205.2	HBA-LI, HBA-LI, HYD-Ar
Hypo5	1.918	0.84	143.5	117.3	208.7	HBA-LI, HBA-LI, HBA-LI, HYD-Ar
Hypo6	1.960	0.83	146.1	114.7	214.5	HBA-LI, HBA-LI, HYD-Ar
Hypo7	2.287	0.76	165.8	95.0	218.5	HBA-LI, HBA-LI, Ar
Hypo8	2.279	0.76	168.9	91.9	219.1	HBA-LI, HBA-LI, Ar
Hypo9	2.339	0.75	169.3	91.5	219.1	HBA-LI, HBA-LI, HYD-Ar
Hypo10	2.442	0.72	176.4	84.4	219.4	HBA-LI, HBA-LI, HYD-Ar
Fixed cost	0	1.00	89.9	170.9		
Null cost	3.537	0	260.8	0		

[a] root mean square deviation (RMSD); [b] squared correlation coefficient; [c] overall cost parameter of the PH4 pharmacophore. [d] cost difference between Null cost and total cost of this hypothesis; [e] lowest cost of 49 scrambled runs (Y) at a selected level of confidence of S = 98%. Fixed Cost = 89.9 with RMSD = 0, Null Cost =260.8 with RMSD = 3.537 and Configuration cost = 9,40. [f] HBA (hydrogen-bond Acceptor); HYD (Hydrophobic); HYD-AL (Hydrophobic Aliphatic); HYD-Ar (Hydrophobic Aromatic); Ar (Ring-aromatic). Number of hypotheses with total cost < Hypo1 cost (=130.5): X=0. S=[1-(1 + X)/Y] ×100=[1-(1 + 0)/ (1 + 49)] ×100 = 98%.

3.5. Virtual library

The permutation of the fragments R1 and R2-group on the coumarin skeleton led us to a Table 5 (VL). The 351 R-groups inventoried in Table 5, were fixed instead of the R1 and R2-groups of the COU skeleton to generate the combinatorial library of the size: R1 x R2 = 351 x 351=123,201 analogs. This initial diversity library was generated from building blocks (chemicals) listed in the databases of available chemicals [44]To achieve a drug-compliant molecule library, we put a filter and applied rules such as the Lipinski-of-five rule, which gave us the reduced (VL) which guided us to sample a reduced number of acceptable COU for in silico testing. This method produced 67,949 analogs.

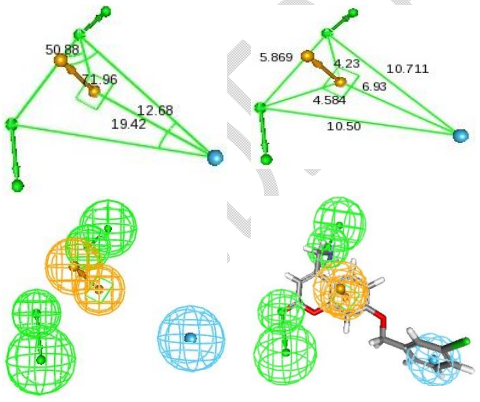

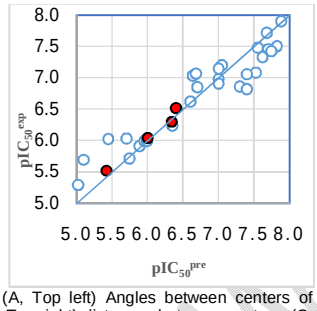

Figure 4. (A, Top left) Angles between centers of pharmacophoric, (B, Top right) distances between centers, (C, Middle left) features coordinates of centers and (D, Middle right) mapping of pharmacophore of MAO-B inhibitor with the most potent molecule COU1. The correlation plot of experimental vs. predicted inhibitory activity is displayed at the left. The features are colored blue for hydrophobic aromatic, green for hydrogen-bond acceptor (HBA) and orange for ring aromatic. The arrows represent the projection for acceptor features. (E, Bottom) Correlation plot of experimental vs predicted inhibitory activity (open square correspond to TS, red square to VS).

3.6. *In Silico* Screening of Library of COUs

The focused library of 67,949 COU analogs (COUa) underwent virtual screening for those structures mapping the 3D-QSAR PH4 model hypo1 of MAO-B inhibition well. 245 COUs mapped to ≥2 features, 50 of them ≥4 features. These best fitting COUa (PH4 hits) were submitted to complexation QSAR model evaluation for predicted IC_{50}^{pre}. The computed rGFE of MAO-B::COUa complex formation ($\Delta\Delta G_{com}$), with $\Delta\Delta H_{MM}$, $\Delta\Delta TS_{vib}$, and $\Delta\Delta G_{sol}$, and IC_{50}^{pre} calculated using Equation B (Table 3) are presented in Table 6.

3.7. Novel COU analogs

The creation of a virtual library was obtained on the basis of chemical information such as conformation, interaction etc of the COUs, which was used for the selection of the appropriate R1-and R2-groups. In order to obtain MAO-B candidates with higher predicted inhibitory activity, we analyzed histogram of R1 and R2-groups among the 50 best fit PH4 hits (Fig.5). The histograms show that the R1 group 159, 96 and 250 were represented with the highest frequency of occurrence (5, 3 and 3 respectively) among the 50 COU hits. The R2-groups most frequently represented in this subset are 280(5) and 335(4) with occurrences of 5 and 4 respectively. The top five scoring virtual hits namely, analogs are 96_271 (IC_{50}^{pre} =20 pM), 14_271 (IC_{50}^{pre} =220 pM), 104_249 (IC_{50}^{pre} =420 pM), 159_90 (IC_{50}^{pre} =525 pM) and 337_279 (IC_{50}^{pre} =562 pM),). They include the following substituents at R_1 positon: 159: 4-(5-amino-1H-pyrazol-1-yl)Ph, 96: 2-thio-3,3-diMebutyl and 250: imino(Ph)Me or at R2 position:280: -Bz-2-F and 335: 3-Hydroxy-Benzyl. These R2-groups, all of which are hydropho-bic rings, have a suitable substituent that explores the depth of the hydrophobic pocket. Unlike R2-groups which includes hydrophobic rings, R1-groups have shown a preference for aliphatic substituents.

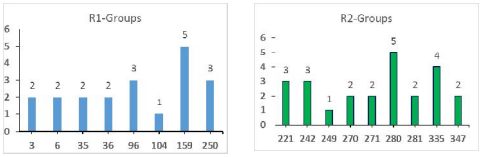

Figure 5: Histograms of frequency of occurrence of individual R-groups in the 50 best selected analogs mapping to four features of PH4 pharmacophore hypothesis Hypo1.

3.8. Pharmacokinetic profile of novel COU analogs

Obtaining a pharmacokinetic profile of MAO-B inhibitors still requires increased research. Presented in Table 7, the ADME of our new analogs, were described earlier by the QikProp program [45] taken from the method of Jorgensen [46]. The fundamental principles of this method are described previously [**Error! Bookmark not defined.**]. Our best analogs are compared with that of drugs used on the market to treat Parkinson's disease. See table 7.

4 DISCUSSIONS

The study of MAO-B complexation and coumarin derivatives carried out by Binda *et al.* [47] can still be explored by QSAR. Exploration of MAO_B-COUx complexes shows that hydrophobic interaction plays a key role in significantly enhancing the expected inhibitory potencies. As shown in Fig.6, there is an enhancement of the E_{int} interaction energy with the amino acids in the hydrophobic pocket surrounded by the following residues: Trp119, Leu164, Leu167, Phe168, Ile198, Ile199, Ile316 and Tyr326 as reported previously [11]. Fig.6 displays in a comparative way this improvement of interaction energy E_{int} with ILE199 and TYR326 known to be the key determinants for binding affinity for the MAO-B inhibitors [6, 7, 8]. This structural model, released during PH4 screening of the virtual library of COUs analogues, led to a significant increase in the efficiency of COUs action in E_{int} breakdown to MAO_B active site residues when comparing the best TS COU1 (ILE199; -5.2 kcal/mol and Tyr326; -5.1 kcal/mol) to two COUs analogs 96-271 (ILE199; -6.9 kcal/mol and Tyr326; -6.1 kcal/mol) and 14-271 (ILE199; -5.9 kcal/mol and Tyr326; -5.6 kcal/mol) and resulting in stabilization of almost 3 kcal/mol for 96-271 and 1 kcal/mol for 14-271.

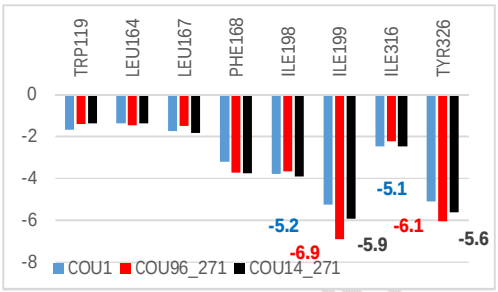

Figure 6 Best two novel COU analogs (the color coding refers to ligands given in legend).

5. CONCLUSIONS

The establishment of the affine function, the PIC50 as a function of the Gibbs energy MAO-B:COUs complex allowed the creation of the solid QSAR model based on the principle of similarity of MAO-B-complexed coumarin ligands, which allows to obtain an affine function between the Gibbs energy and the experimental inhibitory activity. In addition to the QSAR model, we developed a pharmacophore model (PH4), based on the active conformation of the COUs ligands, the 29 series of the assay set and the 4 ligands of the validation set and their experimental inhibitory activities [11]. the information gained from the interaction between MAO-B and the COUs derivatives at the active site allowed us to create a virtual combinatorial library in order to obtain the new COUs analogs. the library screened on the basis of a set of descriptors attached to the ADME sorted by correspondence of analogues to the pharmacophore, allowed selection of a subset of the VL of orally bioavailable COUs. This subset of 50 best virtual hits was submitted to computation of predicted MAO-B inhibitory potencies by the complexation similarity-property principle (SPP) based QSAR model. The best analogs reaches predicted activities in the sub nanomolar concentration range. The best designed COU analogs 96-271 (IC_{50}^{pred} = 0.1 nM), 14-271 (IC_{50}^{pred} = 0.2 nM), 104-249 (IC_{50}^{pred} = 0.4 nM), 337-279 (IC_{50}^{pred} = 0.6 nM) Table 7, are recommended for synthesis and subsequent biological activity evaluation in MAO-B inhibition assays and lead to a discovery of novel potent orally bioavailable antiparkinsonian.

Comment [A7]: Scope of the work should be justified. Limitations of present study should be mentioned.

Table 5 R1-and R2-groups (fragments, building blocks, substituents) used in the design of the initial diversity virtual combinatorial library of coumarin derivatives [27].

Comment [A8]: Table should be placed just after the description.

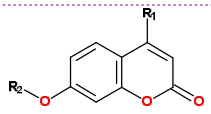

			R-groups [a]		
1	1-ClMe-indolizin-7-yl	2	ET	3	1-F-ET
4	propyl	5	1-Brpropyl	6	Me-thiol
7	1-BrMe	8	1-ClEt	9	1-F-propyl
10	butyl	11	1-F-Me	12	1-BrEt
13	1-Clpropyl	14	1-F-butyl	15	1-Cl-butyl
16	1-Clpentyl	17	hexyl	18	1-Br-hexyl
19	isopentyl	20	6,6-diMeheptyl	21	6-Meheptyl

			R-groups [a]		
22	3,3-diMe-butyl	23	3-Mepentyl	24	6-Meoctyl
25	3-Etpentyl	26	Me-C_3H_5	27	Butyl-C_3H_5
28	Me-C_4H_7	29	Butyl-C_4H_7	30	Me-C_5H_9
31	Butyl-C_5H_9	32	Me-C_6H_{11}	33	Butyl-C_6H_{11}
34	cycloprop-2-en-1-yl	35	Thiophen-2-yl	36	Thiophen-3-yl
37	Furan-2-yl	38	5-Me-thiophen-2-yl	39	3,4,5-triMe-thiophen-2-yl
40	Thiophen-2-ylMe	41	furan-3-ylMe	42	3-Me-thiophen-2-yl
43	3,5-diMe-thiophen-2-yl	44	Furan-2-ylMe	45	2-(thiophen-2-yl)Et
46	4-Me-thiophen-2-yl	47	4,5-diMe-thiophen-2-yl	48	2-(furan-2-yl)Et
49	Thiophen-3-ylMe	50	Ph	51	4-ClPh
52	4-F-Ph	53	4-BrPh	54	p-tolyl
55	3-F-Ph	56	3-ClPh	57	3-BrPh
58	m-tolyl	59	2-F-Ph	60	2-ClPh
61	2-BrPh	62	o-tolyl	63	4-OHPh
64	4-MeOPh	65	4-OH-Bn	66	4-MeO-Bn
67	-Bn	68	4-F-Bn	69	4-Cl-Bn
70	4-Br-Bn	71	4-Me-Bn	72	3,5-diMe-Bn
73	4-((1H-imidazol-2-yl)Me)-Bn	74	aminoMe	75	diClMe
76	2-(1H-imidazol-2-yl)Et	77	2-clpropyl	78	3-Br-2-(thiazol-2-yl)propyl
79	(Furan-3-ylMe)thio	80	diBrMe	81	2-amino-2-ClEt
82	3,3-diBr-3-F-propyl	83	4-(pyridin-3-yl)butyl	84	Cl-F-Me
85	2-(1,3,4-thiadiazol-2-yl)Et	86	2-Br-2-(1,3,4-thiadiazol-2-yl)Et	87	1-Br-3-Clpropyl
88	4-(1H-imidazol-2-yl)butyl	89	4-Cl-3-OHbutyl	90	3-((F-Me)amino)propyl
91	4-OHhexyl	92	6-Br-5-aminohexyl3-((F-Me)amino)propyl	93	4-iodo-3-Mebutyl
94	3-(neopentylamino)propyl	95	5-(Meamino)pentyl	96	2-Thio-3,3-diMebutyl
97	4-Cl-3-Mepentyl	98	6-aminooctyl	99	4-P-3-Etpentyl
100	cycloprop-2-en-1-ylMe	101	(4-Mecyclohexyl)Me	102	4-Et-Bn
103	4-(CF_3)-Bn	104	3,4-diF-Bn	105	3,5-diF-Bn
106	2-Cl-4-F-Bn	107	5-Cl-2-(FMe)-Ph	108	5-Br-2-(FMe)-4-Et-Ph
109	3-Me-2(CF_3)-ph	110	3-F-2(FMe)-ph	111	5-F-2(FMe)-ph
112	3,5-diF-2(FMe)-Ph	113	3-(triFMe)pyridin-2-yl	114	2-(triFMe)pyridin-3-yl
115	3-(triFMe)pyridin-4-yl	116	3-Br-pyridin-2-yl	117	4-MeO-3-(CF_3)pyridin-2-yl
118	4-(CF_3)pyridin-3-yl	119	2-(CF_3)Ph	120	EtO
121	2-(6-Et-3,6-dihydro-2H-pyran-2-yl)EtO	122	4-(2-F-Pyrrol-1-yl)ph	123	4-(4-F-1H-Pyrazol-1-yl)ph
124	4-(3-F-1H-Pyrazol-1-yl)ph	125	4-(4,5-diF-1H-pyrazol-1-yl)Ph	126	4-(3,4,5-triF-1H-pyrazol-1-yl)Ph
127	4-(3,4-diF-1H-pyrazol-1-yl)Ph	128	4-(3,5-diF-1H-pyrazol-1-yl)Ph	129	4-(3-Br-1H-pyrazol-1-yl)Ph
130	4-(4-Br-1H-pyrazol-1-yl)Ph	131	4-(5-Br-1H-pyrazol-1-yl)Ph	132	4-(4,5-diBr-1H-pyrazol-1-yl)Ph
133	4-(3,4-diBr-1H-pyrazol-1-yl)Ph	134	4-(3,5-diBr-1H-pyrazol-1-yl)Ph	135	4-(3,4,5-triBr-1H-pyrazol-1-yl)Ph
136	4-(5-Me-1H-pyrazol-1-yl)Ph	137	4-(4-Me-1H-pyrazol-1-yl)Ph	138	4-(3-Me-1H-pyrazol-1-yl)Ph
139	4-(3,4-diMe-1H-pyrazol-1-yl)Ph	140	4-(4,5-diMe-1H-pyrazol-1-yl)Ph	141	4-(3,5-diMe-1H-pyrazol-1-yl)Ph
142	4-(3,4,5-triMe-1H-pyrazol-1-yl)Ph	143	4-(3-iodo-1H-pyrazol-1-yl)Ph	144	4-(4-iodo-1H-pyrazol-1-yl)Ph
145	4-(5-iodo-1H-pyrazol-1-yl)Ph	146	4-(4,5-iodo-1H-pyrazol-1-yl)Ph	147	4-(3,4,-diiodo-1H-pyrazol-1-yl)Ph
148	4-(3,4,5-triiodo-1H-pyrazol-1-yl)Ph	149	4-(3,5-diiodo-1H-pyrazol-1-yl)Ph	150	4-(3-Cl-1H-pyrazol-1-yl)Ph
151	4-,4-Cl-1H-pyrazol-1-yl)Ph	152	4-(5-Cl-1H-pyrazol-1-yl)Ph	153	4-(4,5-diCl-1H-pyrazol-1-yl)Ph
154	4-(3,5-diCl-1H-pyrazol-1-yl)Ph	155	4-(3,4-diCl-1H-pyrazol-1-yl)Ph	156	4-(3,4,5-triCl-1H-pyrazol-1-yl)Ph
157	4-(3-amino-1H-pyrazol-1-yl)Ph	158	4-(4-amino-1H-pyrazol-1-yl)Ph	159	4-(5-amino-1H-pyrazol-1-yl)Ph
160	4-(4,5-diamino-1H-pyrazol-1-yl)Ph	161	4-(3,5-diamino-1H-pyrazol-1-yl)Ph	162	4-(3,4-diamino-1H-pyrazol-1-yl)Ph
163	4-(3,4,5-triamino-1H-pyrazol-1-yl)Ph	164	4-(3-Me-1H-pyrazol-1-yl)Ph	165	4-(4-Me-1H-pyrazol-1-yl)Ph
166	4-(5-Me-1H-pyrazol-1-yl)Ph	167	4-(4,5-diMe-1H-pyrazol-1-yl)Ph	168	4-(3,5-diMel-1H-pyrazol-1-yl)Ph
169	4-(3,4-diMe-1H-pyrazol-1-yl)Ph	170	4-(3,4,5-triMe-1H-pyrazol-1-yl)Ph	171	4-(5-Et-1H-pyrazol-1-yl)Ph
172	4-(4-Et-1H-pyrazol-1-yl)Ph	173	4-(5-Et-4-Me-1H-pyrazol-1-yl)Ph	174	4-(5-Et-3,4-diMe-1H-pyrazol-1-yl)Ph
175	4-(5-(Me-Me)-1H-pyrazol-1-yl)Ph	176	4-(5-(Me-Me)-4-Me-1H-pyrazol-1-yl)Ph	177	4-(4,5-di(Me-Me)-1H-pyrazol-1-yl)Ph
178	4-(4,5-di(Me-Me)-3-Me-pyrazol-1-yl)Ph	179	4-(5-aminothio-1H-pyrazol-1-yl)Ph	180	4-(4-aminothio-1H-pyrazol-1-yl)Ph
181	4-(4-(aminothio)-5-ME-1H-pyrazol-1-yl)Ph	182	4-(4,5-bis(aminothio)-1H-pyrazol-1-yl)Ph	183	bisPh-4-yl
184	4-(5H-tetrazol-5-yl)Ph	185	4-(Imidazol-1-yl)Ph	186	4-([1,2,4]triazol-1-yl)Ph
187	4-(tetrazol-1-yl)Ph	188	4-(thiophen-2-yl)Ph	189	4-(pyridin-2-yl)Ph

	R-groups [a]				
190	4-(pyrazine-2-yl)Ph	191	4-(pyrimidin-2-yl)Ph	192	4-(pyridazin-3-yl)Ph
193	4-(piperazin-1-yl)Ph	194	3H-Indol-2-yl	195	7H-purin-8-yl
196	1,8a-dihydro-indolizin-2-yl	197	isoquinolin-6-yl	198	quinolin-6-yl
199	cyclopenta-2,4-dienecarbonyl	200	2-Mecyclopenta-2,4-dienecarbonyl	201	2-F-cyclopenta-2,4-dienecarbonyl
202	2-amino-cyclopenta-2,4-dienecarbonyl	203	2-Mecyclopenta-2,4-dienecarbonyl	204	3-Mecyclopenta-2,4-dienecarbonyl
205	2,3-diMecyclopenta-2,4-dienecarbonyl	206	2-Clcyclopenta-2,4-dienecarbonyl	207	3-Clcyclopenta-2,4-dienecarbonyl
208	2,3-diClcyclopenta-2,4-dienecarbonyl	209	3-Brcyclopenta-2,4-dienecarbonyl	210	2-Brcyclopenta-2,4-dienecarbonyl
211	2,3-diBrcyclopenta-2,4-dienecarbonyl	212	2-iodocyclopenta-2,4-dienecarbonyl	213	3-iodocyclopenta-2,4-dienecarbonyl
214	2,3-dilcyclopenta-2,4-dienecarbonyl	215	amino(cyclopenta-2,4-dien-1-yl)Me	216	amino(2-F-cyclopenta-2,4-dien-1-yl)Me
217	amino(2,3-diF-cyclopenta-2,4-dien-1-yl)Me	218	amino(2-Me-cyclopenta-2,4-dien-1-yl)Me	219	amino(2,3-diMe-cyclopenta-2,4-dien-1-yl)Me
220	NH_2Me(2,3-diMecyclopenta-2,4-dien-1-yl)Me	221	NH_2Me(2-Me-cyclopenta-2,4-dien-1-yl)Me	222	NH_2Me(3-Me-cyclopenta-2,4-dien-1-yl)Me
223	NH_2Me(3-F-cyclopenta-2,4-dien-1-yl)Me	224	NH_2Me(2-F-cyclopenta-2,4-dien-1-yl)Me	225	NH_2Me(2,3-F-cyclopenta-2,4-dien-1-yl)Me
226	NH_2F(2,3-diMe-cyclopenta-2,4-dien-1-yl)Me	227	NH_2F(2-Me-cyclopenta-2,4-dien-1-yl)Me	228	NH_2F(3-Me-cyclopenta-2,4-dien-1-yl)Me
229	NH_2F(3-F-cyclopenta-2,4-dien-1-yl)Me	230	NH_2F(2,3-diFcyclopenta-2,4-dien-1-yl)Me	231	NH_2F(2,3-diClcyclopenta-2,4-dien-1-yl)Me
232	NH_2F(2-Clcyclopenta-2,4-dien-1-yl)Me	233	NH_2F(3-Clcyclopenta-2,4-dien-1-yl)Me	234	NH_2F(3-Brcyclopenta-2,4-dien-1-yl)Me
235	NH_2F(2,3-diBrcyclopenta-2,4-dien-1-yl)Me	236	NH_2F(2-Brcyclopenta-2,4-dien-1-yl)Me	237	NH_2(2-carbamoylcyclo penta-2,4-dien-1-yl)Me
238	NH_2(3-carbamoylcyclo penta-2,4-dien-1-yl)Me	239	NH_2(3-F-2carbamoylcyclopenta-2,4-dien-1-yl)Me	240	NH_2(3-Cl-2-carbamoylcyclopenta-2,4-dien-1-
241	NH_2(3-NH_2-2-carbamoylcyclopenta-2,4-dien-1-	242	2-carbamoylPh-$HCOO^-$	243	3-carbamoylPh-$HCOO^-$
244	4-carbamoylPh-$HCOO^-$	245	2-MePh-$HCOO^-$	246	3-MePh-$HCOO^-$
247	4-MePh-$HCOO^-$	248	2,3-diMePh-$HCOO^-$	249	(2-carbamoylPh)(imino)Me
250	imino(Ph)Me	251	(3-carbamoylPh)(imino)Me	252	4-carbamoylPh(imino)Me
253	2-MePh(imino)Me	254	2,3-diMePh(imino)Me	255	3-MePh(imino)Me
256	4-MePh(imino)Me	257	2-FPh(imino)Me	258	3-FPh(imino)Me
259	3-BrPh(imino)Me	260	2-BrPh(imino)Me	261	2-ClPh(imino)Me
262	3-ClPh(imino)Me	263	(3-ClPh)(Br-imino)Me	264	(3-BrPh)(Br-imino)Me
265	(3-ClPh)(Cl-imino)Me	266	(2-ClPh)(Cl-imino)Me	267	(2-MePh)(-imino)Me
268	imino(2-(CF_3)Ph)Me	269	imino(3-(CF_3)Ph)Me	270	3-formylbenzamide
271	2-formylbenzamide	272	4-formylbenzamide	273	-Bz-2-thiol
274	-Bz-2,3-diMe	275	-Bz-3-Me	276	-Bz-4-Me
277	-Bz-2-Me	278	-Bz-2-(CF_3)	279	-Bz-3-(CF_3)
280	-Bz-2-F	281	NH_2(3-Br-2-carbamoylcyclopenta-2,4-dien-1-yl)Me	282	Carbamoyl
283	4-Cl-1H-pyrazol-1-yl	284	4,5-diCl-1H-pyrazol-1-yl	285	5-Cl-1H-pyrazol-1-yl
286	3-Cl-1H-pyrazol-1-yl	287	3-Br-1H-pyrazol-1-yl	288	4-Br-1H-pyrazol-1-yl
289	5-Br-1H-pyrazol-1-yl	290	4,5-diBr-1H-pyrazol-1-yl	291	3,4,5-triBr-1H-pyrazol-1-yl
292	4-Me-1H-pyrazol-1-yl	293	4,5-diMe-1H-pyrazol-1-yl	294	5-Me-1H-pyrazol-1-yl
295	5-iodo-1H-pyrazol-1-yl	296	4-iodo-1H-pyrazol-1-yl	297	3-iodo-1H-pyrazol-1-yl
298	3,4-diI-1H-pyrazol-1-yl	299	3,4,5-triiodo-1H-pyrazol-1-yl	300	3,4-diF-1H-pyrazol-1-yl
301	3-F-1H-pyrazol-1-yl	302	1,3-diF-1H-pyrazol-1-yl	303	1-F-1H-pyrazol-1-yl
304	1-F-1H-pyrazol-2-yl	305	3-amino-1H-pyrazol-1-yl	306	4-amino-1H-pyrazol-1-yl
307	5-amino-1H-pyrazol-1-yl	308	5-Me-1H-pyrazol-1-yl	309	5-Et-1H-pyrazol-1-yl
310	4-Me-1H-pyrazol-1-yl	311	4,5-diMe-1H-pyrazol-1-yl	312	5-(Me-Me)-1H-pyrazol-1-yl
313	4-Me-5-(Me-Me)-1H-pyrazol-1-yl	314	5-(H_2N-thio)-4-Me-1H-pyrazol-1-yl	315	4,5-bis(aminothio)-1H-pyrazol-1-yl
316	4,5-bis(H_2N-thio)-3-Me-1H-pyrazol-1-yl	317	5-Et-3-Me-1H-pyrazol-1-yl	318	pyridazin-3-yl
319	pyridazin-4-yl	320	pyrimidin-4-yl	321	1,3,5-triazin-2-yl
322	pyrimidin-2-yl	323	pyrazin-2-yl	324	Cyclohexyl
325	piperazin-1-yl	326	tetrahydropyridazin-1(2H)-yl	327	piperazin-1-yl
328	3-Cl-benzyl	329	Me-amino-Me	330	2-amino-Et
331	Acetic acid	332	Benzoic acid	333	2-F-2-(1-Me-ureido)-acetamide
334	4-tert-butyl-benzoic acid	335	3-Hydroxy-Benzyl	336	Benzyloxy-(3-br-propyl)NH_2-Me
337	Propionic acid	338	dipropylaminomethyl	339	(3-br-propyl)ph-amino Me
340	[(Bromo-Me-Me sulfanyl-amino)-Me]	341	Bis(Me-Me)-amino Me	342	Me-urea
343	hydroxyaminomethyl	344	urea	345	(cyclohexyl-3-Et-pentyl)-amino-Me
346	Acetamide	347	3-Cl-Me-benzyl	348	3-Cl-5-Me-benzyl
349	3-propyl-benzyl	350	3-bromomethyl-benzyl	351	hydroxy

[a] All fragments were used for substitutions in the R_1 and R_2 positions.

Table 6 rGFE $\Delta\Delta G_{com} = \Delta\Delta H_{MM} + \Delta\Delta G_{sol} - \Delta\Delta TS_{vib}$ for the top scoring 50 virtual COU analogs. For analog name the R1 and R2 indexes of substituent numbers come from Table 5.

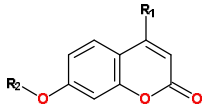

N°	Designed[a] Analogues	M_w[a]	$\Delta\Delta H_{MM}$[b]	$\Delta\Delta G_{sol}$[c]	$\Delta\Delta TS_{vib}$[d]	$\Delta\Delta G_{com}$[e]	IC_{50}^{pred}[f] [nM]
-	COU1	329.8	0.0	0.0	0.0	0.0	13[g]
1	298-335	492.1	-4.2	4.2	-4.0	4.0	144.4
2	204-280	408.4	-29.9	25.4	-4.8	0.3	21.7
3	337-279	406.3	-20.5	7.6	-6.0	-6.9	0.6
4	346-347	371.1	-2.6	0.3	-1.7	-0.6	13.7
5	250-280	387.4	-10.9	7.3	-4.2	0.6	25.6
6	344-347	372.8	-6.9	1.3	-2.7	-2.8	4.4
7	247-335	420.4	-11.7	11.3	-5.9	5.5	303.5
8	250-221	422.5	-5.3	9.7	-1.3	5.7	336.9
9	306-70	412.2	-1.6	2.4	-0.9	1.7	45.1
10	344-106	344.8	-0.2	2.1	-4.4	6.3	465.1
11	301-273	382.4	-1.5	2.9	-2.8	4.2	156.1
12	250-91	393.4	-12.5	8.4	-1.6	-2.5	5.2
13	275-222	455.6	-5.9	14.5	0.1	8.5	1367.2
14	273-196	429.5	-7.3	8.8	-2.5	4.0	142
15	35-280	366.4	-6.9	3.9	-3.1	0.1	19.9
16	238-85	410.5	-20.2	12.2	-2.9	-5.0	1.4
17	243-250	428.4	-10.7	11.4	-6.1	6.8	602.4
18	1-238	463.9	-17.8	18.6	-0.2	1.1	33.2
19	6-278	380.3	-0.1	2.5	-5.0	7.4	798.6
20	6-339	434.4	1.3	2.6	0.0	3.9	136
21	47-272	419.5	2.3	3.9	-2.6	8.9	1719
22	71-333	413.4	-17.9	9.2	-1.7	-6.8	0.6
23	85-280	396.4	-0.1	-0.4	-5.5	4.9	231.7
24	2-242	353.3	-2.3	5.7	-1.4	4.8	214.6
25	14-271	383.4	-25.6	15.5	-1.3	-8.7	0.2
26	96-271	425.5	-17.9	6.1	1.3	-13.2	0.1
27	79-205	430.5	-19.5	12.4	-7.7	0.6	25.9
28	35-335	350.4	-6.6	4.5	0.4	-2.4	5.4
29	96-270	425.5	-13.9	8.3	0.5	-6.2	0.8
30	102-163	467.5	-42.4	47.8	-1.3	6.7	555.5
31	294-267	377.4	7.0	-0.9	-0.1	6.2	439.6
32	104-249	434.4	-20.6	8.5	-4.5	-7.5	0.4
33	89-242	431.8	-2.7	3.0	-2.1	2.4	63
34	91-64	368.4	-21.5	24.8	1.7	1.5	40.7
35	163-281	564.4	-21.1	24.6	-2.1	5.6	316.6
36	96-281	493.4	-17.2	16.9	3.5	-3.8	2.7
37	277-239	434.4	2.9	2.8	-3.6	9.3	2089.3
38	36-240	414.9	-1.0	6.4	-2.9	8.2	1202.3
39	3-221	365.4	6.4	3.4	2.7	7.0	660
40	3-216	319.3	0.6	4.1	-0.2	4.9	230
41	37-92	406.3	8.2	2.5	4.1	6.6	530
42	36-242	407.4	-9.9	7.6	-3.7	1.5	40
43	314-335	413.5	5.5	1.1	-1.9	8.5	1420
44	201-280	394.3	-34.4	24.7	-5.4	-4.2	2.2
45	158-221	476.6	-17.5	12.1	0.3	-5.6	1.1
46	159-270	466.5	-26.7	18.7	-5.2	-2.7	4.7
47	159-90	408.4	-25.3	17.3	-0.9	-7.0	0.5
48	159-94	446.5	-21.0	14.8	-0.5	-6.7	0.6
49	159-117	494.4	-16.4	15.4	-6.2	5.2	270
50	159-79	431.5	-17.4	21.6	-4.3	8.4	1370

[a] M_w [$g.mol^{-1}$] is the molecular mass of inhibitors ; [b] $\Delta\Delta H_{MM}$ [$kcal.mol^{-1}$] is the relative enthalpic contribution to the Gibbs free energy change related to enzyme-inhibitor (E:I) complex formation $\Delta\Delta G_{com}$ (for details see footnote pf Table 2); [c] $\Delta\Delta G_{sol}$ [$kcal.mol^{-1}$] is the relative solvation Gibbs free energy contribution to $\Delta\Delta G_{com}$; [d] $\Delta\Delta TS_{vib}$ [$kcal.mol^{-1}$] is the relative(vibrational) entropic contribution to $\Delta\Delta G_{com}$; [e] $\Delta\Delta G_{com}$ [$kcal.mol^{-1}$] is the relative Gibbs free energy change related to the enzyme-inhibitor MAO-B:: COU complex formation $\Delta\Delta G_{com} \cong \Delta\Delta H_{MM} + \Delta\Delta G_{sol} - \Delta\Delta TS_{vib}$; [f] IC_{50}^{pre} is the predicted inhibition potency MAO-B inhibitors calculated from $\Delta\Delta G_{com}$ using correlation B; Table 3; [g] IC_{50}^{exp} [nM] is given for the reference inhibitor COU1 instead of the IC_{50}^{pre}.

Table 7 Predicted ADME-related properties of the best designed COU analogues and known Parkinson agents either in clinical.

COUx[a]	#stars[b]	M_W[c]	S_{mol}[d]	$S_{mol/hfo}$[e]	V_{mol}[f]	RotB[g]	HB_{don}[h]	HB_{acc}[i]	$logP_{o/w}$[j]	$logS_{wat}$[k]	logKHsa[l]	PlogB/B[m]	BIPcaco[n]	#meta[o]	$IC50^{pre}$[p] (nM)	HOA[q]	% HOA[r]
337-279	0	406.3	649.5	109.7	1140.3	4	0	7.5	2.8	-4.4	-0.2	-0.9	319.2	2	0.6	3	87.9
344-347	0	372.8	636.4	123.7	1111.8	5	3	5.2	2.3	-3.6	-0.0	-1.5	57.9	4	4.4	3	87.8
250-91	0	393.4	711.4	214.4	1271.2	10	2	7.7	2.9	-4.7	0.1	-2.1	121.2	2	5.2	3	81.0
238-85	0	410.4	669.2	108.5	1192.7	8	4	8.7	0.8	-3.0	-0.2	-2.1	6.2	8	1.4	2	83.9
71-333	0	413.4	695.4	194.3	1241.0	6	3	7.5	1.1	-2.8	-0.4	-2.1	14.4	4	0.6	2	84.4
14-271	0	383.4	668.2	152.7	1172.1	6	2	7.5	2.5	-4.9	0.0	-1.7	141.2	2	0.2	3	80.2
96-271	0	425.5	699.4	183.9	1272.8	7	2.8	8	2.9	-5.1	0.1	-1.6	145.3	3	0.0	3	82.6
35-335	0	350.4	608.2	29.1	1054.3	4	1	4	3.9	-5.4	0.5	-0.8	629.5	4	5.4	3	100
96-270	0	425.5	705.9	184.0	1282.2	7	2.8	8	2.7	-5.2	0.2	-1.9	85.6	3	0.8	3	85.6
104-249	0	434.4	689.3	35.9	1237.9	7	3	6.5	3.5	-5.5	0.3	-1.5	154.6	2	0.4	3	86.6
96-281	0	493.4	711.8	215.2	1307.8	9	4.8	7.2	2.6	-4.0	0.1	-1.3	31.6	7	2.7	2	69.0
Rasagiline	2	173.3	417.1	210.6	675.1	4	1.5	1.5	2.3	-1.3	-0.1	0.5	1562.4	5		3	100
Lazabemide	0	199.6	400.9	74.6	643.5	4	3	4.5	0.1	-0.6	-0.5	-0.3	96.9	3		2	63.1
Safinamide	0	302.3	575.7	168.0	998.0	7	3	4.7	1.8	-1.6	-0.3	-0.3	139.2	6		3	75.9

[a] designed TKI analogues (Table 6) and known anti tuberculosis; [b] drug-likeness, number of property descriptors (24 of the full list of 49 QikProp descriptors, ver. 6.5, release 139) that fall outside the *range of values for 95% of known drugs*; [c] molar mass in [$g.mol^{-1}$] (*range for 95% of drugs: 130–725 g_mol*$^{-1}$) [48]; [d] total

solvent-accessible molecular surface, in (Å2) (probe radius 1.4 Å) (*300–1000 Å2*); [e] hydrophobic portion of the solvent-accessible molecular surface, in (Å^2) (*0–750 Å^2*); [f] total volume of the molecule enclosed by solvent-accessible molecular surface, in (Å^3) (*500–2000 Å^3*); [g] number of rotatable non-trivial (not CX3), non-hindered (not alkene, amide, small ring) bonds (*0–15*); [h] estimated number of hydrogen bonds that would be donated by the solute to water molecules in an aqueous solution. Values are averages taken over a number of configurations, so they can assume non-integer values (*0.0–6.0*); [i] estimated number of hydrogen bonds that would be accepted by the solute from water molecules in an aqueous solution (*2.0–20.0*); [j] logarithm of the partition coefficient between the n-octanol and water phases (*-2 to 6.5*); [k] logarithm of predicted aqueous solubility, logS. S in (mol.dm^{-3}) is the concentration of the solute in a saturated solution that is in equilibrium with the crystalline solid (*-6.0 to 0.5*); [l] logarithm of the predicted binding constant to human serum albumin (*-1.5 to 1.5*); [m] logarithm of the predicted brain/blood partition coefficient (*-3.0 to 1.2*); [n] predicted apparent Caco-2 cell membrane permeability on the Boehringer–Ingelheim scale in [nm.s^{-1}] (*<25 poor, >500 nm s^{-1} great*); [o] number of likely metabolic reactions (*1–8*); [p] predicted inhibition constants IC_{50}^{pre} of designed TKIs vs. *Mtb* Thymidylate kinase.; [q] human oral absorption (*1 = low, 2 = medium, 3 = high*); [r] percentage of human oral absorption in the gastrointestinal tract (*<25% = poor, >80% = high*); * star in any column indicates that the property descriptor value of the compound falls outside *the range of values for 95% of known drugs*.

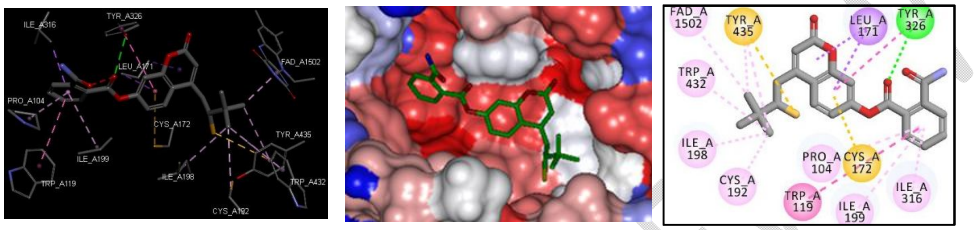

96-271

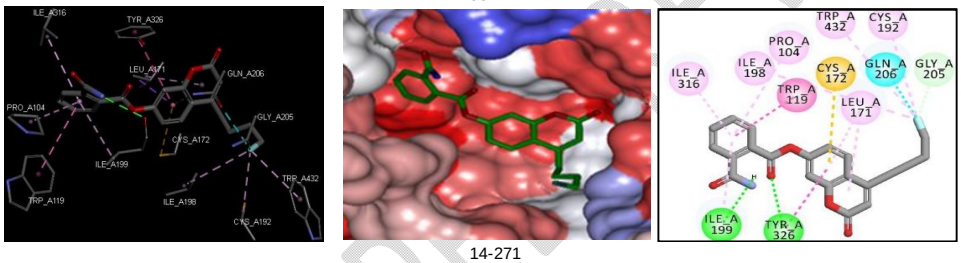

14-271

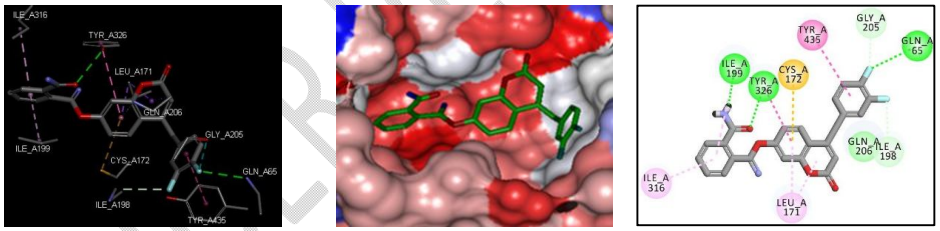

104-249

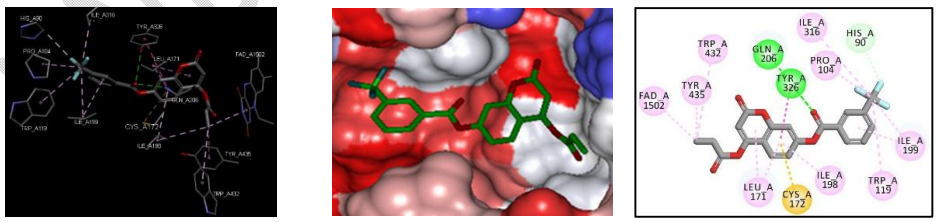

337-279

Figure 7: The virtual hit 96-271, 14-271, 104-249, 337-279. The most active designed COU analogs at the active site of MAO-B (3D). 2D schematic interaction diagram of the most active designed COU analogs. Connolly Surface of the active site of MAO-B for 4 best active designed COU analogs. The binding site surface is colored according to residue hydrophobicity: red = hydrophobic, blue = hydrophilic and white = intermediate

ABBREVIATIONS

2D : Two-dimensional
3D : Three-dimensional
ADME : Absorption, distribution, metabolism, and excretion
MAO-B : Monoamine Oxidase B
hMAO-B : Human Monoamine Oxidase B
hMAO-A : Human Monoamine Oxidase A
COUx : Training set of Coumarins derivatives
COU : Coumarins derivatives
$\Delta\Delta G_{com}$: Relative complexation GFE
GFE : Gibbs free energy
VL : Virtual Library
VCL : Virtual Combinatorial Library
$\Delta\Delta G_{sol}$: Relative solvation GFE
HBA : Hydrogen bond Acceptor
HBD : Hydrogen bond Donor
HMM : Enthalpy component of GFE
IC50 : Half-maximal inhibitory concentration
K_i : inhibitory concentration
HOA : Human oral absorption
HYD : Hydrophobic
HYDA : Hydrophobic Aliphatic
MM : Molecular mechanics
MM-PB : Molecular mechanics–Poisson–Boltzmann
PDB : Protein Data Bank
PH4 : Pharmacophore
QSAR : Quantitative structure–activity relationships
RMSD : Root-mean square deviation
D.S. 2.5 : Discovery Studio 2.5
TS : Training set
VS : Validation set

References

1. Strolin B. M., Tipton K. F., Whomsley R. Amine oxidases and monooxygenases in the in vivo metabolism of xenobiotic amines in humans: has the involvement of amine oxidases been neglected? *Fundam Clin Pharmacol*. **2007**; 21(5):467-80. doi: 10.1111/j.1472-8206.2007.00498.x
2. Shih J. C., Chen K., Ridd M. J., Monoamine oxidase: from genes to behavior. *Annu Rev Neurosci.* **1999**; 22:197-217. doi:10.1146/annurev.neuro.22.1.197.
3. Edmondson D. E., Binda C., Wang J., Upadhyay A. K., Mattevi A. Molecular and mechanistic properties of the membrane-bound mitochondrial monoamine oxidases. *Biochem*. **2009**, 48, 4220-4230. https://doi.org/10.1021/bi900413g.
4. Bortolato M., Chen K., Shih J. C., Monoamine oxidase inactivation: from pathophysiology to therapeutics. *Adv Drug Deliv Rev.* **2008**; 60(13-14): 1527-33. https://doi.org/10. 1016/j.addr.2008.06.002.
5. Lawrence M. S., George P., and Mark A. S., *Chemical Res. Toxicol.* **2008** *21* (1), 172-188 DOI:10.1021/tx700210j.
6. Tsugeno Y, Ito A. A key amino acid responsible for substrate selectivity of monoamine oxidase A and B. *J Biol Chem*. **1997,** 272(22):14033-6. doi: 10.1074/jbc.272.22.14033
7. Hubalek F., Binda C., Khalil A., Li M., Mattevi A., Castagnoli N., & Edmondson D. E. Demonstration of isoleucine 199 as a structural determinant for the selective inhibition of human monoamine oxidase B by specific reversible inhibitors. *J.Biol. Chem*. **2005**, 280, 15761-15766.
8. Geha R. M., Rebrin I., Chen K., & Shih J. C. Substrate and inhibitor specificities for human monoamine oxidase A and B are influenced by a single amino acid. *J. Biol*. **2001**, 276, 9877-9882.
9. Li M., Binda C., Mattevi A., & Edmondson D. E. Functional role of the 'aromatic cage' in human monoamine oxidase B: Structures and catalytic properties of Tyr 435 mutant proteins. *Biochemistry* **2006**, 45, 4775-4784.
10. Binda C., Wang J., Pisani L., Caccia C., Carotti A., Salvati P., Edmondson D., Mattevi A. Structures of human monoamine oxidase B complexes with selective noncovalent inhibitors : safinamide and coumarin analogs. *J. Med. Chem*. **2007**, 50, 5848-5852.
11. Leonardo P., Giovanni M., Teresa F. M., Orazio N., Francesco L., Marco C., Carla C., Patricia S., Ramon S.O., Estefania M. A., Celine P., & Angelo C. Discovery of a Novel Class of Potent Coumarin Monoamine Oxidase B Inhibitors. **2009**, *J. Med. Chem*. 52, 6685-6706. https://doi.org/10. 1021/jm9010127.
12. Youdim M. B.H., Gross A. and Finberg J.P.M. Rasagiline [N-propargyl-1R(+)-aminoindan], a selective and potent inhibitor of mitochondrial monoamine oxidase B. **2001**, British *J. Pharmacol.* 132, 500-506. DOI:10.1038/sj.bjp.0703826
13. Saura J., Kettler R., Da Prada M., and Richards J. G. Quantitative Enzyme Radioautography with 3H-Ro 41-I 049 and 3H-Ro 19-6327 in vitro: Localization and Abundance of MAO-A and MAO-B in Rat CNS, Peripheral Organs, and Human Brain. **1992**, *J. Neurosci,* 12(5): 1977-1999. DOI: 10.1523/JNEUROSCI.12-05-01977.1992
14. Binda C., Wang J., Pisani L., Caccia C., Carotti A., Salvati P., Edmondson D. E., and Mattevi A. Structures of Human Monoamine Oxidase B Complexes with Selective Noncovalent Inhibitors: Safinamide and Coumarin Analogs. **2007**, *J. Med. Chem*., 50, 5848-5852. DOI: 10.1021/jm070677y
15. Berman H. M., Westbrook J., Feng Z., Gilliland G., Bhat T. N., Wessig H., Shindyalov I. N., Bourne P. E. The protein data bank. *Nucl. Acids Res*. **2000**, 28, 235-242.
16. Discovery Studio molecular modeling and simulation program version 2.5, Accelrys, Inc., San Diego, CA, 92121, USA, **2009.**
17. Owono Owono L. C., Keita M., Megnassan E., Frecer V. & Miertus S. Design of Thymidine Analogues Targeting Thymidilate Kinase of Mycobacterium tuberculosis. *Tuberculosis research and treatment*, **2013**, 670836. https://doi.org/10.1155/2013/670836.
18. Frecer V., Miertus S., Tossi A. & Romeo D. Rational design of inhibitors for drug-resistant HIV-1 aspartic protease mutants. *Drug Des. Discov*., **1998**,15(4), 211-231.
19. Frecer V., Miertus S. Interactions of ligands with macromole-cules: rational design of specific inhibitors of aspartic protea-se of HIV-1. *Macromol Chem Phys*; **2002,** 203: 1650–1657 https://doi.org/10.1002/1521-3935(200207)203:10/11<1650::AID-MACP1650>3.0.CO;2-E
20. Frecer V., Berti F., Benedetti F. & Miertus S. Design of peptidomimetic inhibitors of aspartic protease of HIV-1 containing -Phe Psi Pro- core and displaying favourable ADME-related properties. *J. Mol. Graph Model*, **2008**, 27 (3), 376-387. https://doi.org/10.1016/j.jmgm.2008. 06.006.
21. Dali B., Keita M., Megnassan E., Frecer V. & Miertus S. Insight into selectivity of peptidomimetic inhibitors with modified statine core for plasmepsin II of plasmodium falciparum over human cathepsin D. Chem. *Biol. Drug Des*. **2012**, 79 (4), 411-430. https://doi.org/10.1111/ j.1747-0285.2011.01276.x.
22. Megnassan E., Keita M., Bieri C., Esmel A., Frecer V. & Miertus S. Design of novel dihydroxynaphthoic acid inhibitors of plasmodium falciparum lactate dehydrogenase. *Med. Chem*. **2012**, 8(5), 970-984.
23. Keita M., Kumar A., Dali B., Megnassan E., Siddiqi M. I., Frecer V. and Miertus S. Quantitative Structure-activity relationships and design of thymine-like inhibitors of thyme-dine monophosphate kinase of *Mycobacterium tuberculosis* with favourable pharmacokinetic profiles. *RSC Adv.*, **2014**, 4(99), 55853-55866. https://doi.org/10.1039/c4ra06917j.
24. Owono Owono L. C., Ntie-Kang F., Keita M., Megnassan E., Frecer V. and Miertus S. Virtually Designed Triclosan-Based Inhibitors of Enoyl-Acyl Carrier Protein Reductase of Mycobaterium tuberculosis and of Plasmodium falciparum. *Mol. Inform.*, (2015) 34(5), 292-307. https://doi.org/10.1002/minf.201400141.
25. Kouassi A. F., Kone M., Keita M., Esmel A., Megnassan E., N'Guessan Y. T., & Miertus S. Computer-Aided Design of orally Biovailable

pyrrolidine Carboxamide Inhibitors of Mycobacterium turberculosis with Favorable Pharmaco-kinetic Profiles. *Int. J. Mol. Sci*, (**2015**). 16 (12), 29744-29771. https://doi.org/10.3390/ ijms161226196.

26. Allangba K. N. P. G., Keita M.,Kre N'Guessan R., Megnassan E., Vladimir F., Miertus S. Virtual design of novel *Plasmodium falciparum* cysteine protease falcipain-2 hybrid lactone–chalcone and isatin–chalcone inhibitors probing the S2 active site pocket, *Journal of Enzyme Inhibition and Medicinal Chemistry*, **2019**, 34:1, 547-561. https://doi.org/10.1080/14756366. 2018.1564288

27. Kouman K. C., Keita M., N'Guessan K. R., Owono Owono L.C., Megnassan E., Vladimir F. & Miertus S., Structure-Based Design and *in silico* Screening of Virtual Combinatorial Library of Benzamides Inhibiting 2-trans Enoyl-Acyl Carrier Protein Reductase of *Mycobacterium tuberculosis* with Favorable Predicted Pharmacokinetic Profiles. *Int. J. Mol. Sci.*, **2019**, 20, 4730. https://doi.org/10.3390/ijms20194730.

28. N'Guessan, H., Soro, I., Keita, M. and Megnassan, E. "Design and *in silico* Screening of Combinatorial Library of New Herbicidal Analogs of Cycloalka[d]quinazoline-2,4dione-Benzoxazinones Inhibiting Protoporphyrino-gen IX Oxidase", *J. Pharm. Res. Int*., **2022**, 34(56), pp. 42–61. doi:10.9734/jpri/2022/v34i567251

29 Bernard, D. A. M., Keita, M., Bisseyou, Y. B. M., Esmel, A. and Megnassan, E. "Computer-assisted Design of Novel Polyketide Synthase 13 of Mycobacterium tuberculosis Inhibitors Using Molecular Modeling and Virtual Screening", *J. Pharm. Res. Int.*, **2022**, 34(56), pp. 12–41. doi:10.9734/jpri/2022/v34i567250.

30. Bieri C., Esmel A., Keita M., Owono Owono LC., Dali B., Megnassan E., Frecer V., Miertus S. « Structure-Based Design and Pharmacophore-Based Virtual Screening of Combinatorial Library of Triclosan Analogues Active against Enoyl-Acyl Carrier Protein Reductase of Plasmodium falciparum with Favourable ADME Profiles », *Int. J. Mol. Sci.*, **2023,** 24, (8): 6916. doi:10.3390/ijms24086916.

31. Kone M., N'Guessan H., N'Gouan A. J., M-Koblavi F., Megnassan E. Computer-aied Design of New Hydroxamic Acid Derivatives Targeting the Plasmodium falciparum M17 Metallo-aminopeptidase with Favorable pharmcokinetic Profile. *Int. J. Pharm. Sci. and Drug Res*. **2023**, 15(3) : 356-375. https://doi.org/10.25004/ IJPSDR.2023.150317

32 Ziki E., Akonan L., Kouman K.C., Dali B., Megnassan E.,Kakou-Yao R., Tenon A. J., Frecer V., and Miertus S., Virtual Design of Novel CoumarinylSubstituted Sulfonamide Inhibitors of Carbonic Anhydrase II as Potential Drugs against Glaucoma. *J. Pharm. Res. Int.***, 2023**, 35(24), pp. 10-33. DOI: 10.9734/JPRI/2023/ v35i247424

33. Maple, J.R.; Hwang, M.-J.; Stockfisch, T.P.; Dinur, U.;Waldman, M.; Ewig, C.; Hagler,. A. Derivation of class II force fields. I. Methodology and quantum force field for the alkyl functional group and alkane molecules. *J. Comput. Chem*, **1994**, 15, 162–182.

34. Gilson M., & Honig B. The inclusion of electrostatic hydration energies in molecular mechanics calculations. *J Computer Aided Mol Des*, **1991**, 5(1), 5-20.

35. Rocchia W., Sridharan S., Nicholls A., Alexov E., Chiabrera A. & Honig B. Rapid grip-based construction of the molecular systems and geometric objects. *J Comput Chem*, **2002**, 23(1), 128-137. https://doi.org/ :10.1002/jcc.1161.

36. Böttcher C. J. F. HSTORICAL INTRODUCTION *Theory of Electric Polarization* (second Edition **1973**, (pp.1-8) Amsterdam Elsevier.

37. Miertus S., Scrocco E. & Tomosi J. Electrostatic interaction of a solute with a continuum. A direct utilization of AB initio molecular potentials for the prevision of solvent effects. *Chemical physics*, **1981**, 55(1) 117-129. https://doi.org/:10.1016/0301-0104(81) 85090-2.

38. Copeland R. A., Lombardo D., Giannaras J., & Decicco C. P. Estimating KI values for tight binding inhibitors from dose-reponse plots. *Bioorganic & Medicinal Chemistry letters*, **1995**, 5(17), 1947-1952. https:// doi.org/:10.1016/0960-894X(95)00330-V.

39. Li H., Sutter J., Hoffmann R., Pharmacophore Perception, Development and use in Drug Design, Güner O. F., Ed.; International University line : san Diego, CA, USA, **2000**; PP. 171-189.

40. Binda C., Li M., Hubalek F., Restelli N., Edmondson D. E., Mattevi A.. Insights into the mode of Inhibition of Human Mitochondrial Monoamine Oxidase B from high-Resolution Crystal Structures. *Proc. Natl. Acad. Sci. U.S.A*., **2003**, 100, 9750-9755.

41. Binda C., Hubalek F., Li M., Herzig Y., Sterling J., Edmondson D. E., Mattevi A.. Crystal Structures of MAO B in Complex with Four Inhibitors of the N-Propargyl-aminoindan Class. *J. Med. Chem.*, **2004**, 47, 1767-1774.

42. William J.A., David R. B,. Steered Molecular Dynamics Simulations Reveal Important Mechanisms in Reversible Monoamine Oxidase B Inhibition *Biochemistry*, **2011**, 50, 6441-6454. https://doi.org/ 10.1021/bi200446w.

43 John, S.; Thangapandian, S.; Sakkiah, S.; Lee, K.W. Potent BACE-1 inhibitor design using pharmacophore modeling, *in silico* screening and molecular docking studies. *BMC Bioinform*. **2011**, 12, S28.

44. Available Chemicals Directory, version 95.1, MDL Information Systems, San Leandro, CA. **2003**. Available online: https://cds3.dl.ac.uk/cds/cds.html .

45. QikProp, version 3.7, release 14; X Schrödinger, LLC: New York, NY, **2014**

46 Jorgensen W. L., Duffy E. M. Prediction of drug solubility from Monte Carlo simulations. *Bioorg. Med. Chem. Let*. **2000**, 10, 1155-1158.

47. Binda C., Newton-Vinson P., Hubálek F., Edmonson D. E. & Mattevi A. Structure of human monoamine oxidase B, a drug target for the treatement of neurological disorders. *Nat. Struc. Biol.*, **2001**, 9(1), 22-26. https://doi.org/:10.1038/nsb732.

48. Duffy, E. M., & Jorgensen, W. L. Prediction of Properties from Simulations: Free Energies of Solvation in Hexadecane, Octanol, and Water. *J. Am. Chem. Soc.*, **2000**, *122*(12), 2878-2888. https://doi:10.1021/ ja993663t.